Journal of MATERIALS RESEARCH

Article
DOI:10.1557/s43578-023-00951-9

Incorporation of chondroitin sulfate into macroporous bacterial cellulose scaffold for improved bioactivity

Quanchao Zhang[1,2,b)], Bingbing Zhong[1,2,b)], Yichuan Zhang[1,2,b)], Zhiwei Yang[1,2], Xiangbo Zhu[1,2], Jie Wang[1,2], Honglin Luo[1,2,3,a)], Yizao Wan[1,2,3,a)]

[1] *Jiangxi Key Laboratory of Nanobiomaterials, Institute of Advanced Materials, East China Jiaotong University, Nanchang 330013, China*
[2] *School of Materials Science and Engineering, East China Jiaotong University, Nanchang 330013, China*
[3] *School of Materials Science and Engineering, Tianjin University, Tianjin 300350, China*
[a)] Address all correspondence to these authors. e-mails: hlluotju@126.com; yzwantju@126.com
[b)] These authors have contributed equally to this work.

Received: 9 December 2022; accepted: 15 February 2023; published online: 2 March 2023

Lack of bioactivity limits the applications of bacterial cellulose (BC) in biomedical fields. In this study, we report the facile preparation of a macroporous BC (PBC)/chondroitin sulfate (CS) scaffold using the ex situ method by adding CS solution into the suspension of BC fragments followed by crosslinking with 1-ethyl-3(3-dimethyl aminopropyl) carbodiimide (EDC) and N-hydroxysuccinimide (NHS) and freeze drying. The PBC/CS scaffold was characterized for morphology, physicochemical properties, cell behavior, and capability of inducing mineral deposition. Results show that the PBC/CS scaffold presents improved mechanical properties, cell adhesion, and proliferation over the PBC scaffold. Moreover, the presence of CS greatly enhances the deposition of minerals on the PBC/CS scaffold, an indicator of bioactivity. The present study provides a simple methodology for improving the bioactivity of BC and the results of the present work suggest that the PBC/CS scaffold has potential for use in bone tissue engineering.

Introduction

Since the first report on bacterial cellulose (BC) wound dressings [1], rapid progress has been made in the last decades in the field of BC biomaterials. These advancements are triggered by the development of nanotechnology due to its unique nanostructure including nano-scaled fibers and pores as well as many striking physiochemical properties, such as high mechanical strength, large water holding ability, high-chemical purity, good moldability, to name a few [2–4]. The non-woven BC nanofibrous microstructure closely resembles the structure of native extracellular matrix (ECM), making it suitable for tissue engineering scaffolds. To this end, many previous studies have demonstrated its versatility in constructing various scaffolds or replacements such as wound dressings, bone regeneration, small-diameter blood vessel, and dura mater [2, 5–8]. Despite these advantages, critical drawbacks of BC greatly hinder its practical applications in biomedical fields, namely insufficient bioactivity, non-biodegradability, and dense structure (native BC has pore sizes of 0.02–10 μm [9–11]). Mitigating these limitations has long been the focus of BC biomaterials for more than 20 years. For instance, to make it biodegradable, oxidation using sodium periodate is a common approach [12–14]. To create large pores, various methods have been developed such as phase separation, sodium chloride salt leaching, insertion of placeholders, and post-processing using laser patterning and many others [11, 12, 15–17]. To endow it with favorable bioactivity, in situ (modifications are done while the BC pellicle is formed by adding bioactive materials in the culture medium of BC) and ex situ (modifications are conducted after the BC pellicle is formed by immersing BC in solutions of bioactive materials or compounding with them) modifications have been developed to meet requirements of different tissue engineering applications [18, 19]. Compared with the in situ method, the ex situ one is more versatile and can easily control the concentration of bioactive materials in the final BC-based biomaterials. To date, numerous bioactive materials have been reported such as collagen, gelatin, chitosan, starch, polycaprolactone, polyvinyl alcohol, and glycerol [18–21].

Besides those bioactive materials, chondroitin sulfate (CS), extensively present in the ECM of cartilage, bone, and skin, attracts much attention. CS is essentially a sulphated glycosaminoglycan with a protein core and polysaccharide branches

containing carboxylic (-COO^-) and sulfate ester (-SO_4^{2-}) groups, which make it highly negative [22, 23]. Earlier studies suggested that CS could control cellular migration, attachment, and proliferation, playing an important role in promoting tissue regeneration [24]. Therefore, CS has been widely used as a scaffold material [22, 24–29], and more importantly, it is often incorporated into tissue engineering scaffold [26]. For instance, Chen et al. claimed that a CS-modified polylactic acid/gelatin scaffold promoted cartilage regeneration and inhibited inflammation [26]. Xu et al. developed a scaffold consisting of chitosan, strontium, and CS and found that the CS-incorporated scaffold showed positive effects on downregulation of inflammation and osteoclastogenesis related mRNA expressions while demonstrating a significant increase in the expression level of bone morphogenetic protein-2 [29]. Pezeshki-Modaress et al. developed gelatin/CS nanofibrous scaffolds using electrospinning technique for skin tissue engineering and significantly accelerated wound healing was demonstrated [24]. Interestingly, CS was also used by de Olyveira and co-workers to modify BC via the in situ modification method [30, 31], but the cell behavior of the CS-added BC was not investigated.

Unlike previous reports, in this work, we prepared a CS-incorporated macroporous BC scaffold by the ex situ route (Fig. 1, for details see Section of *preparation of PBC and PBC/CS scaffolds* in Materials and methods Part). The morphology and physicochemical properties of the macroporous BC/CS (PBC/CS) scaffold were assessed. The cell behavior and in vitro bioactivity were also evaluated and the roles of CS were determined.

Results and discussion

Characterization of scaffolds

The morphology of the PBC and PBC/CS scaffolds is shown in Fig. 2(a) and (b), respectively. The insets show the digital photos of cylindrical PBC and PBC/CS scaffolds. It is noted that the PBC and PBC/CS scaffolds demonstrate similar interconnected macroporous structure. The high-magnification SEM images reveal that the pore walls consist of a large number of nanofibers for both PBC and PBC/CS scaffolds. However, the average pore sizes are different, being 170 ± 7.2 μm and 148.4 ± 1.4 μm for PBC and PBC/CS scaffolds, respectively [Fig. 2(c) and (d)]. The pore size of the PBC scaffold changes in a wider range from 50 to 300 μm than the PBC/CS scaffold (70–230 μm). It is believed that pristine BC is a densely packed fibrous structure and its pore size (maximum 10 μm) is too small to allow the ingrowth of cells into the scaffold after in vivo implantation [7, 12, 15, 32]. The average pore size of the PBC and PBC/CS scaffolds is appropriate for bone regeneration as the pore size of 100–200 μm is believed to be able to induce significant ingrowth of bone tissue [33].

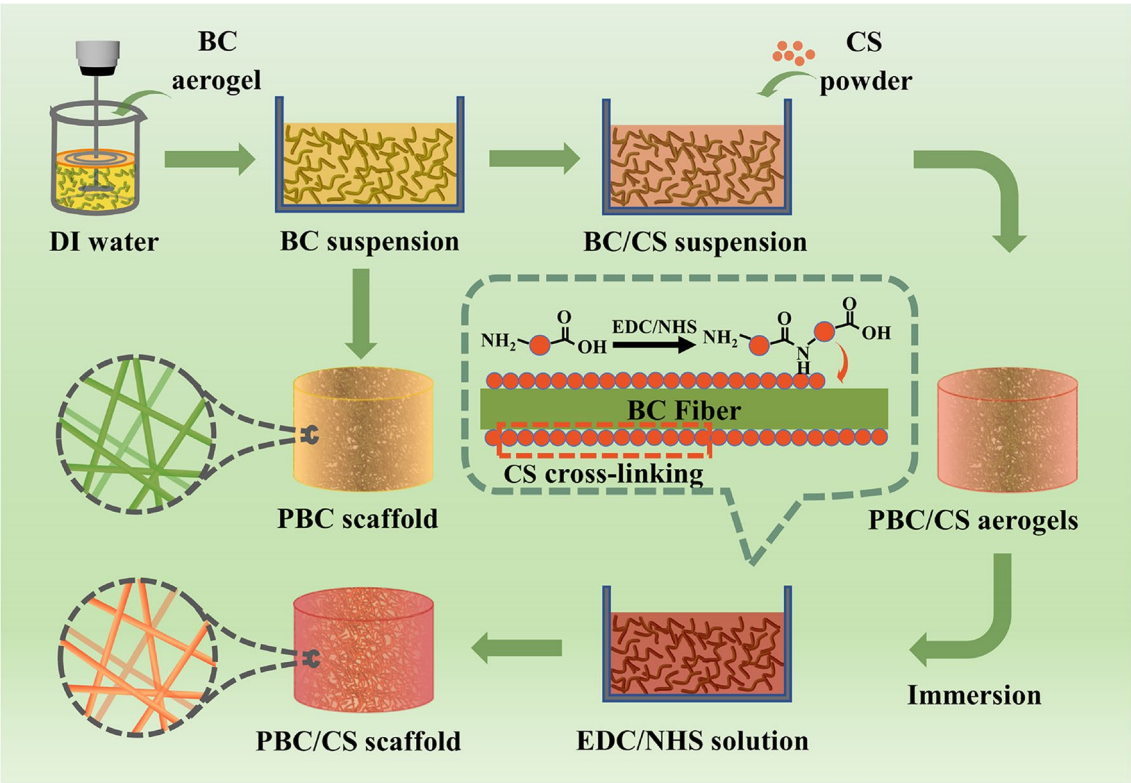

Figure 1: The schematic diagram showing the preparation process of PBC and PBC/CS scaffolds.

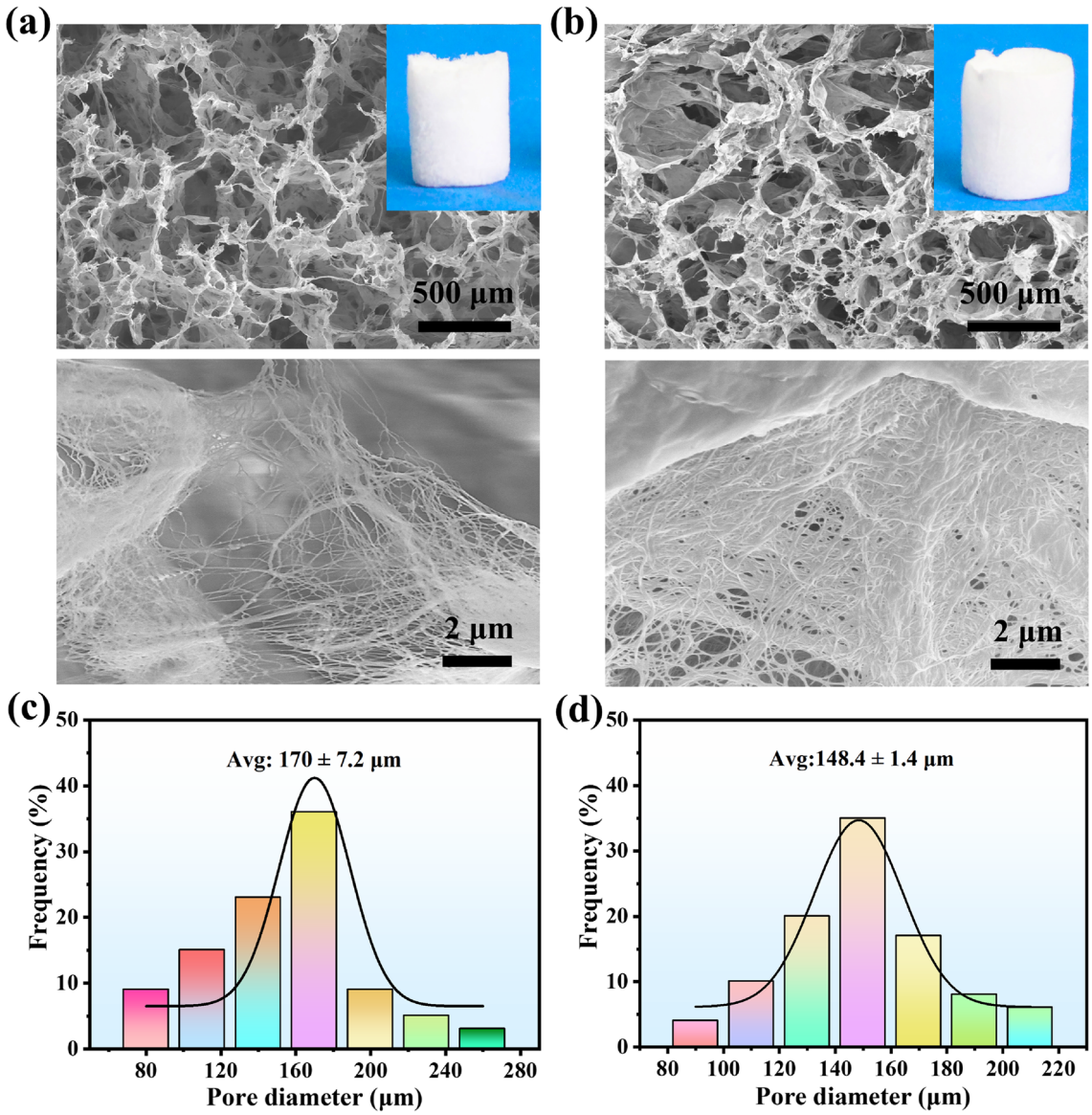

Figure 2: SEM images (a and b) and pore size distribution (c and d) of PBC (a and c) and PBC/CS (b and d) scaffolds. Insets show the digital photos of PBC and PBC/CS scaffolds.

Figure 3(a) shows the FTIR spectra of the PBC and PBC/CS materials. The peaks at 3500–3200 and 2943 cm^{-1} are attributed to -OH stretching vibration and C-H asymmetric stretching vibration in BC cellulose, respectively [34–37]. In the spectrum of the PBC/CS material, the strong peak at 1607 cm^{-1} is caused by C = O stretching vibration, the peak at 1224 cm^{-1} is due to S = O stretching vibration (attributed to the negatively charged -SO_4^{2-} groups in CS) [24], and the peak at 855 cm^{-1} is C-O-S stretching vibration in CS [24]. It is noted that the C = O peak shifts to 1640 cm^{-1}, suggesting possible hydrogen bonding between CS and PBC.

The surface chemistry of the PBC and PBC/CS materials was determined by XPS [Fig. 3(b)–(e)]. Figure 3(b) shows the XPS survey spectra. Besides elements C and O in the PBC material, elements N and S are noted in the PBC/CS material, indicating the successful compounding of CS and PBC. Additionally, the atomic contents of C and O in PBC were 60.13% and 39.87%, respectively; while the atomic contents of C, O, N and S in PBC/CS were 64.88%, 30.01%, 3.36% and 1.75%, respectively. When compraed with PBC, the atomic ratio of O/C in PBC/CS decreased from 0.67 to 0.46, further suggesting the successful incorporation of CS in PBC. The high-resolution C 1 s spectrum of the PBC material [Fig. 3(c)] shows the presence of three peaks at 284.6, 286.8, and 288.3 eV, which are due to C–C, C-O, and O-C-O of cellulose, respectively [38]. As shown in Fig. 3(d), in addition to the above three characteristic peaks

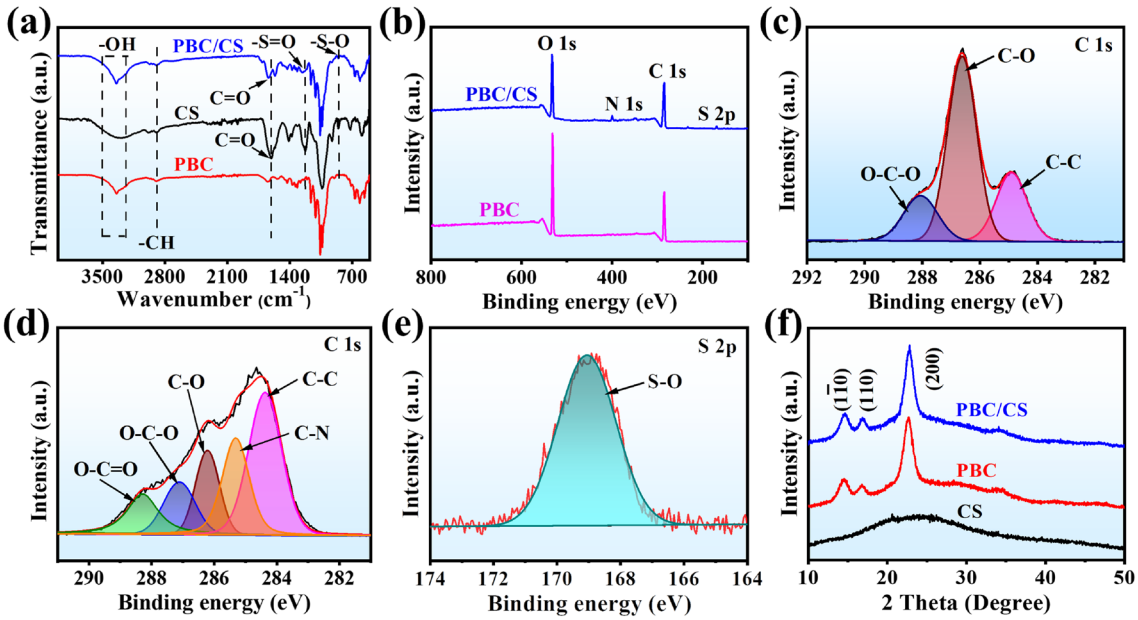

Figure 3: (a) FTIR spectra of PBC and PBC/CS materials; (b-e) XPS spectra of PBC and PBC/CS materials: (b) Survey spectra, (c) High-resolution C 1 s spectrum of PBC, (d) High-resolution C 1 s spectrum of PBC/CS, (e) High-resolution S 2p spectrum of PBC/CS; (f) XRD patterns of PBC and PBC/CS materials.

of C–C, C-O, and O-C-O, the C-N peak (285.6 eV) and O-C = O peak (288.7 eV) are also observed in the PBC/CS material, corresponding to the -COOH and -CH-NH- in CS, respectively [39]. Additionally, the high-resolution S 2p spectrum [Fig. 3(e)] of the PBC/CS material shows the presence of S–O (168.9 eV), which corresponds to the SO_4^{2-} groups in CS [39]. These results indicate the successful synthesis of the PBC/CS by the simple mixing method.

Figure 3(f) shows the XRD patterns of the CS, PBC, and PBC/CS materials. The CS material shows a typical wide peak at around 22˚, suggesting it is a semi-crystalline material, consistent with previous reports [40, 41]. As expected, the PBC and PBC/CS materials show three characteristic peaks at 14.5˚, 16.8˚, and 22.8˚, corresponding to the (1$\bar{1}$0), (110), and (200) diffraction planes of type I cellulose [42, 43], respectively. This result indicates that the crystal structure of the PBC was not changed by intense stirring and EDC/NHS treatment.

Thermal stability and Porosity analysis

The thermal stability of the PBC and PBC/CS materials was analyzed by thermogravimetric analysis (TGA) [Fig. 4(a)]. The comparison of the two TGA curves of reveals that the addition

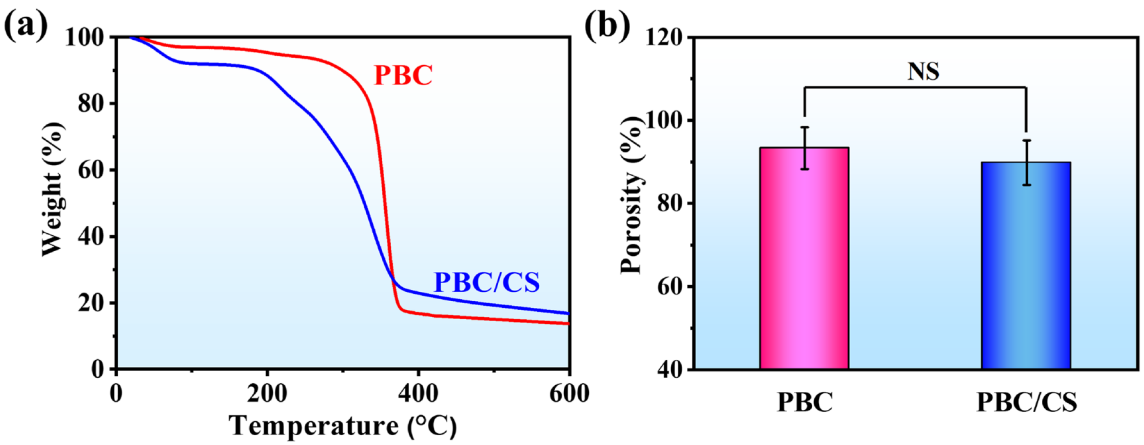

Figure 4: TGA curves (a) and porosity (b) of PBC and PBC/CS scaffolds. NS represents insignificant difference between PBC and PBC/CS, $p > 0.05$, n = 3.

of CS lowers the onset temperature of thermal degradation while increasing the residual weight of PBC.

The porosity measurement [Fig. 4(b)] reveals a total porosity of 89.8% and 93.3% of PBC/CS and PBC, respectively, which is not a significant difference ($p > 0.05$).

Mechanical properties of scaffolds

Compressive properties are important for tissue engineering scaffolds. Therefore, the mechanical properties of the PBC and PBC/CS scaffolds were tested under compressive loadings (Fig. 5). Figure 5(a) reveals that the compressive stress–strain curves of the PBC and PBC/CS scaffolds include three distinct regimes, i.e., a linear elastic regime, a collapse plateau regime, and a densification regime. These curves are typical for the so-called "open-cell foam" [44–46]. According to previous reports [47, 48], we determined the compressive stresses of the PBC/CS scaffold at 20, 40, and 60% strain, which are 11.3, 21.7, and 41.1 kPa, respectively, which are significantly higher than those (2.3, 3.8, and 7.9 kPa) of the PBC scaffold. Note that the strength values of PBC/CS scaffolds were lower than the values of traditional BC based scaffolds [49–51] as the macroporous structure and the break of the continuous connected fibrous structure for the PBC/CS scaffolds. However, they were still higher than those of the reported BC based scaffolds with the similar microstructure and preparation procedure [52, 53]. Furthermore, the compressive modulus of the PBC/CS scaffold (61.4 kPa) also shows seven times higher than that of the PBC scaffold (7.7 kPa) [Fig. 5(b)]. The scaffolds should provide mechanical and structural support to sustain the size and shape of engineered tissue [54–57]. Therefore, the PBC/CS scaffold showed better mechanical properties than PBC scaffold and was more desirable for using as bone repair scaffold.

In vitro behavior

Cell viability assays

Although de Olyveira et al. reported the preparation of BC/CS via the in situ modification [30, 31], they did not assess the cell behavior. In this work, to determine how CS affects the biocompatibility of the PBC scaffold, cell studies were conducted. Fluorescent images [Fig. 6(a)] obtained with CLSM reveal continuous and robust growth of MC3T3-E1 osteoblasts on the surface and into the scaffolds and few dead cells are found, indicating that the two materials have good biocompatibility. However, the cell density is different between the PBC and PBC/CS scaffolds; more cells are observed throughout the PBC/CS scaffolds, indicating its superior biocompatible to the PBC. This finding can be further confirmed by the quantitative results presented in Fig. 6(b). At each time point, significant differences in cell viability (indicated by absorbance) are noted between the two scaffolds ($p < 0.05$ on day 1 and $p < 0.01$ on day 4 and 7). These differences indicate the significant role of CS in improving the proliferation of MC3T3-E1 osteoblasts.

Cellular morphology

To observe cell morphology, SEM analysis was conducted. Figure 7(a) reveals that the cells are round on the PBC scaffold while the cells spread well with numerous pseudopodia on the PBC/CS scaffold and thus the cell spreading area is significantly larger ($p < 0.01$), as shown in Fig. 7(b). These results further confirm better biocompatibility of the PBC/CS scaffold than the PBC scaffold.

In vitro biological assessment

Apart from cell biocompatibility, we compared the bioactivity of the PBC and PBC/CS scaffolds by in vitro bioactivity

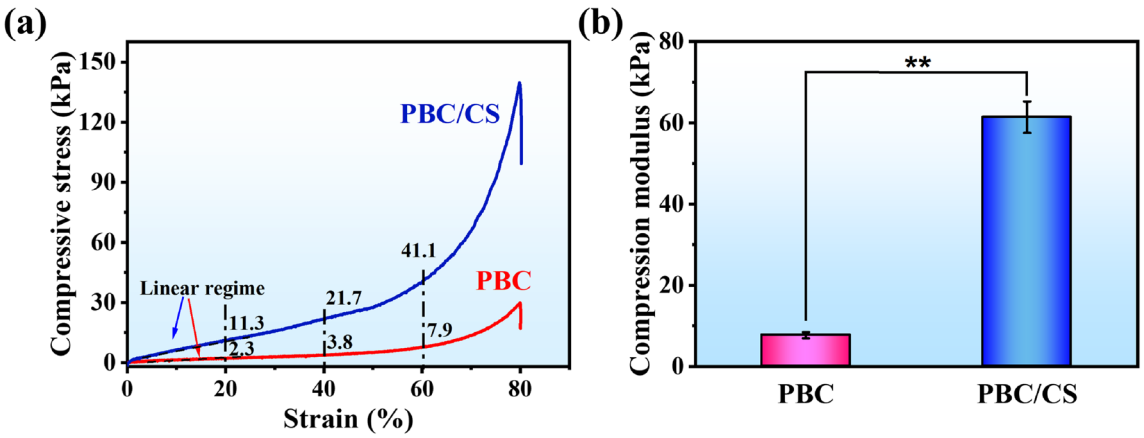

Figure 5: The compressive properties of the PBC and PBC/CS scaffolds. (a) Stress–strain curves, (b) Compressive modulus. The double asterisks (**) indicate statistically significant differences for $p < 0.01$, n = 6.

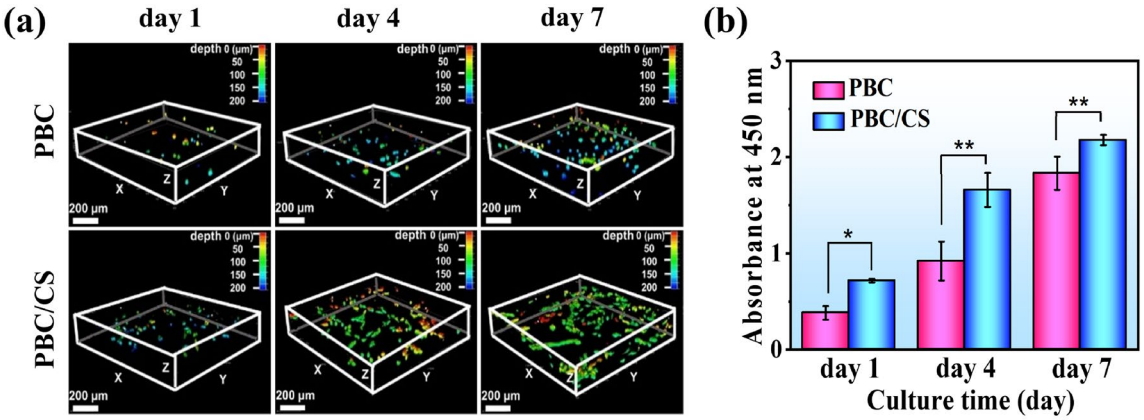

Figure 6: (a) Fluorescent images of FDA and PI stained MC3T3-E1 cells after seeding on the PBC and PBC/CS scaffolds for 1, 4, and 7 days. (b) CCK-8 assay results. The asterisk (*) indicates statistically significant differences for $p < 0.05$, double asterisks (**) indicate statistically significant differences for $p < 0.01$, n = 4.

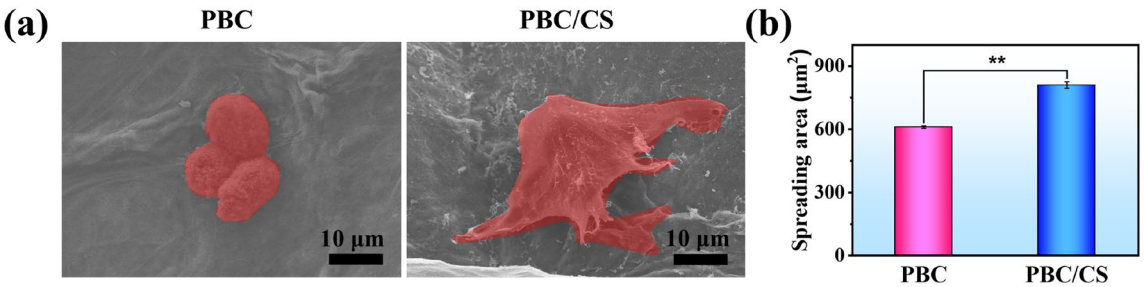

Figure 7: (a) SEM images of MC3T3-E1 cells after seeding on the PBC and PBC/CS scaffolds for 7 days. (b) Cell spreading area on two scaffolds. The double asterisk (**) indicates statistically significant differences for $p < 0.01$, n = 4.

assessment. After immersion in 1.5 × SBF for 7 days, there are fewer and smaller deposits on the surface of the PBC scaffold (Fig. 8(a) as compared with the PBC/CS scaffold [Fig. 8(b)]. The EDS analysis result [Fig. 8(c)-(d)] shows the presence of Ca and P with a Ca/P atomic ratio of 1.19 and 1.62 for the PBC and PBC/CS scaffolds, respectively.

To further characterize the deposits on the PBC and PBC/CS scaffolds, XRD analysis was conducted. As shown in Fig. 8(e), after soaking for 7 days, besides the aforementioned three characteristic peaks of the PBC scaffold, two new peaks located at 31.9° and 45.7° are observed, which are due to the (211) and (203) crystal planes of hydroxyapatite (HAp), which confirms the formation of the Ca-P phase. Moreover, the peak intensity in the XRD pattern of the PBC/CS scaffold is stronger than that in PBC. This indicates that the PBC/CS scaffold is more bioactive than the PBC, which is similar to the result of SEM.

The deposition (including nucleation and growth) of Ca-P minerals is mainly dependent on surface functional groups of the substrate materials [58]. Many previous studies suggested that the –OH groups on BC nanofibers are active to induce mineral formation [59–61]. It is believed that the nonionic -OH groups on the BC absorb the Ca^{2+} through ionic–dipolar interaction followed by Ca-P growth around these trapped ions [62], as illustrated in the proposed schematic diagram (Fig. 9). In the case of PBC/CS, there are a large number of -COO^- and -SO_4^{2-} groups, which may react with Ca^{2+} through ionic interaction (Fig. 9). Compared with ionic–dipolar interaction, ionic interaction is much stronger, which can explain the higher bioactivity of PBC/CS than PBC.

Although further in vitro and in vivo studies are required, the present work suggests that the BC-based scaffold with good bioactivity can be achieved by simply adding CS into the BC suspension followed by freeze drying, which is important to the development and applications of BC-based biomaterials.

Conclusions

The PBC/CS scaffold was prepared by adding CS solution to the suspension of BC fragments followed by EDC/NHS crosslinking and lyophilization. Mechanical tests demonstrated that the incorporation of CS greatly increased the mechanical properties (compressive strength and modulus) of the PBC scaffold. The

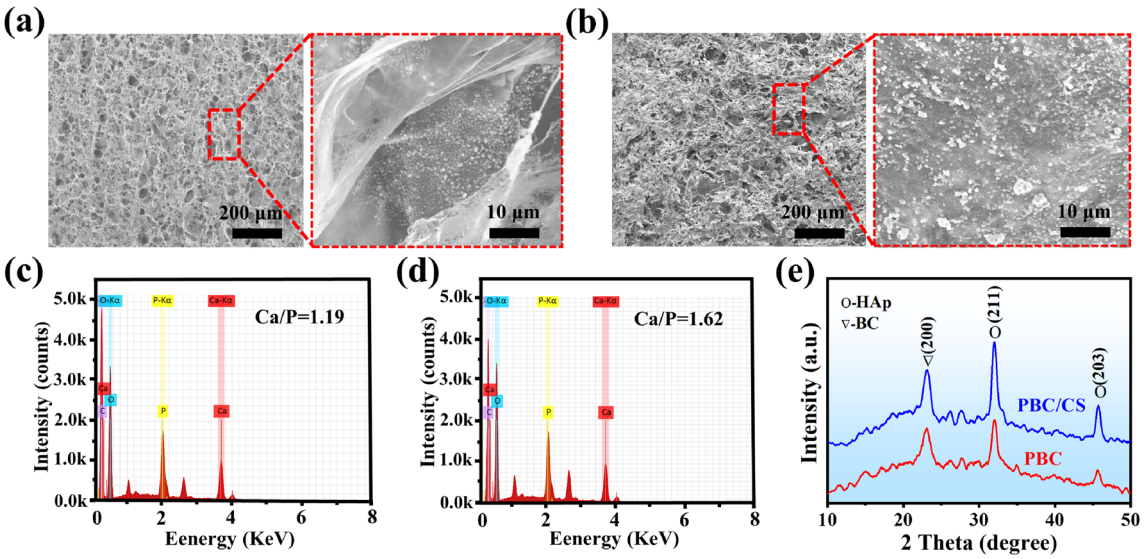

Figure 8: SEM images (a and b) and EDS spectra (c and d) of the deposits grown on the PBC and PBC/CS scaffolds after soaking in 1.5×SBF for 7 days. (E) XRD patterns of the PBC and PBC/CS scaffolds after soaking in 1.5×SBF for 7 days.

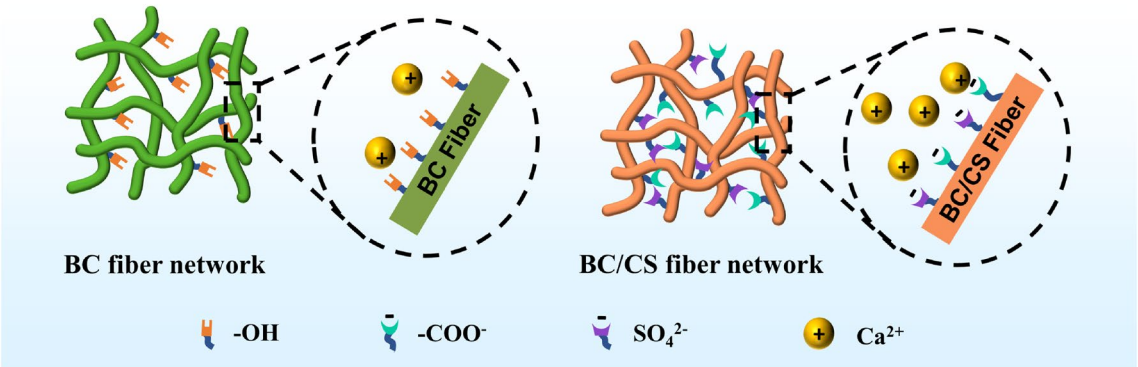

Figure 9: A schematic diagram showing the deposition of Ca^{2+} onto the surfaces of PBC and PBC/CS.

PBC/CS scaffold showed porous microstructure with average pore size of *ca*. 148 μm. In addition, it showed improved cell proliferation. More importantly, the presence of CS in the PBC/CS scaffold substantially enhanced the capability of inducing Ca-P deposition, suggesting improved in vitro bioactivity over the PBC scaffold. The PBC/CS scaffold may be an appropriate material for bone tissue engineering.

Materials and methods

Materials

The reagents for BC production including glucose (BR, > 95%), yeast extract (BR), tryptone (BR), and Na_2HPO_4 (AR, ≥ 99%) were purchased from Acros, New Jersey, USA. CS (AR, 95%), 1-ethyl-3-(3-dimethylaminopropyl) carbodiimide hydrochloride (EDC, AR, 98%), and N-hydroxysuccinimide (NHS, AR, 98%) were purchased from Sigma Chemical Company (Shanghai, China). MC3T3-E1 cells (mouse embryo osteoblasts) were provided by Cell Bank of Chinese Academy of Sciences (Shanghai, China). Minimum Eagle's medium (α-MEM, BR, Gibco), fetal bovine serum (FBS, BR, Gibco), and trypsin (BR, 0.25%) were purchased from Pufei Bio-Technology Co., Ltd., Shanghai, China. Fluorescein diacetate (FDA, BR, 97%) and propidium iodide (PI, BR, 94%) were provided by Aladdin Biochemical Technology Co., Ltd., Shanghai, China. All other chemicals were of analytical grade and purchased from Sinopharm Chemical Reagent Co., Ltd., Shanghai, China.

Preparation of BC aerogel

The recipe of the culture medium (pH 4.5) used in this study was reported in our previous works [42, 63, 64], which included

2.5% (w/v) glucose, 0.75% (w/v) yeast extract, 1% (w/v) tryptone, and 1% (w/v) Na_2HPO_4. Prior to incubation, the culture medium was sterilized at 121 °C for 30 min, followed by static incubation at 30 °C for 7 days using *Komagataeibacter xylinus* X-2 as the bacterial strain. Upon completion of the incubation and subsequent soaking in deionized (DI) water at 90 °C for 2 h, boiling in a 0.5 M NaOH solution for 15 min, and washing with DI water until a neutral pH was achieved, the purified BC pellicles were obtained. The BC aerogel was formed by the following steps. First, the BC pellicles were soaked in tertiary butanol for 3 times (2 h each time) to remove the DI water, then the BC aerogel was formed by freeze drying at – 20 °C for 24 h and lyophilization at – 50 °C for 36 h.

Preparation of PBC and PBC/CS scaffolds

The preparation process of the PBC and PBC/CS scaffolds was displayed in Fig. 1. The obtained BC aerogel was cut into small fragments (3 mm × 3 mm), added to DI water, and soaked overnight for complete water swelling. A high-speed homogenizer (FJ200-SH, Shuaijia Electron Sci. and Tech. Co., Ltd., Shanghai, China) was used to disintegrate the BC aerogel at 12,000 rpm for 30 min, yielding the BC suspension containing 0.5 wt.% BC. To prepare the PBC/CS scaffold, CS powder was added to the obtained BC suspension to yield BC/CS suspension with a CS concentration of 0.25 wt.%. The BC and BC/CS suspensions were poured into 48-well plates separately, pre-frozen at – 20 °C overnight, and freeze-dried at – 50 °C for 48 h. The resultant scaffolds were crosslinked with ethanol solution containing EDC (5 g/L) and NHS (3 g/L) for 24 h under darkness. The scaffolds were washed with DI water to remove excess CS and salt, frozen at – 20 °C overnight, and finally freeze-dried at – 80 °C for 48 h, yielding the PBC and PBC/CS scaffolds.

Characterization

The PBC and PBC/CS scaffolds were sputter-coated with gold and analyzed with scanning electron microscopy (SEM, FEI Nano 430, FEI Company, USA) coupled with energy dispersive spectrometer (EDS) for element analysis. The average pore diameter of the two scaffolds was determined by measuring at least 200 randomly selected pores [65]. X-ray diffraction (XRD) analysis was conducted to determine the crystalline structure of the scaffold materials using a Rigaku D/max 2500 X-ray diffractometer (Rigaku Corporation, Japan) using Cu-K_α radiation ($\lambda = 0.154$ nm). The surface chemistry was evaluated using Fourier transform infrared spectroscopy (FTIR, Spectrum two, PerkinElmer Inc., Massachusetts, USA) and the spectra was recorded in a spectral range of 4000–500 cm^{-1} at a resolution of 4 cm^{-1}. X-ray photoelectron spectroscopy (XPS, AXIS Ultra DLD, Japan) was conducted to further determine the surface chemistry and the elemental ratios.

Thermogravimetric (TG) test

The thermal stability of the PBC and PBC/CS scaffolds was analyzed by thermogravimetric analyzer (TG, Pyris1, PerkinElmer, USA), and the 5–10 mg sample was placed in the crucible. In nitrogen atmosphere, the flow rate is 20 mL/min, the heating rate is 10 ℃/min, and the heating range is 50–800 ℃.

Porosity measurement

The liquid displacement method [34] was used to measure the porosity of the scaffolds:

$$\text{Porosity}\ (\%) = (W_b - W_c - W_0)/(W_a - W_c) \times 100\% \quad (1)$$

where W_0 represents the dry weight of the sample before immersion in ethanol, W_a is the weight of the bottle completely filled with ethanol, W_b denotes the weight of the bottle containing ethanol and the sample, excluding the amount of displaced ethanol due to the addition of the sample, and W_c is the weight of the bottle and remaining ethanol after quick removal of the sample.

Mechanical properties

The compressive properties were measured using a microelectromagnetic fatigue testing machine (MUF-1050, Tianjin Care Measure and Control Co., Ltd., Tianjin, China). The samples with a diameter of 10 mm and a height of 10–15 mm were tested at a strain rate of 5 mm/min.

Cell studies

Cell culture and seeding

The MC3T3-E1 cells (passaged to the fourth generation) were incubated in α-MEM solution supplemented with 10% FBS in a humidified incubator with 5% CO_2 at 37 °C. After 3 days incubation, the cells were digested using 1 mL of trypsin (0.25%) for 2 min. The digestion was terminated by adding 5 mL of cell culture medium. Afterwards, the culture medium with the digested cells was centrifuged at 1000 rpm for 5 min and the supernatant was removed. After adding fresh culture medium, the cell suspension was obtained. The cell suspension was co-cultured with sterilized scaffolds in a 48-well tissue culture plate at a cell density of 1×10^4 cells per well. The culture was performed in a humidified incubator with 5% CO_2 at 37 °C

for 1, 4, and 7 days, during which the medium was refreshed every other day.

Cell morphology

The cell morphology was observed with the aforementioned SEM. After incubation for 7 days, the MC3T3-E1 cells were fixed with 2% glutaraldehyde solution at 4 °C for 12 h, dehydrated in a graded series of ethanol (50, 60, 70, 80, 90, 95, and 100%), gold-sputtered, and viewed under SEM.

Cell proliferation

The cell proliferation was evaluated by cell counting kit-8 (CCK-8) assay. The sterilized scaffolds were pre-soaked in α-MEM for at least 12 h and then incubated in 24-well tissue culture plates for 1, 4, and 7 days. Subsequently, the CCK-8 reagent (50 μL, Solarbio, China) was added to each well followed by incubation in darkness for 2 h at 37 °C. The resultant culture medium was transferred to 96-well plates and the absorbance was read at 450 nm using a microplate reader (iMark, Bio Rad, USA).

Live/dead staining

At the end of culture, the cell-scaffold constructs were rinsed with PBS and then stained with FDA and PI reagents. After incubation for another 2 min, the stained cells were observed using a confocal laser scanning microscopy (CLSM, Leica SP8, Heidelberg, Germany).

In vitro bioactivity assessment

The measurement of in vitro bioactivity of the PBC and PBC/CS scaffolds was carried out in 1.5 times simulated body fluid (1.5 × SBF) that was prepared according to Aparecida's report [66]. Briefly, cylindrical scaffolds (diameter 8 mm, height 10 mm) was immersed in 1.5 × SBF in a polyethylene bottle at 37 °C for 7 days. Subsequently, the scaffolds were collected and rinsed with ethanol and dried. The surface morphology and structure of the samples were analyzed by the aforcementioned SEM and XRD, respectively.

Statistical analysis

All experiments were performed in triplicate unless otherwise stated. An SPSS software (SPSS 20, SPSS Inc., Chicago, USA) was used for statistical data analysis and the mean values and standard deviations (SD) were reported. The statistical significance was considered when the p-value was less than 0.05.

Acknowledgments

This work was supported by the National Natural Science Foundation of China (Grant Nos. 31870963, 51973058, and 32160229), the Key Research and Development Program of Jiangxi Province (Grant No. 20192ACB80008), the Key Project of Natural Science Foundation of Jiangxi Province (Grant No. 20202ACBL204013), and the Science and Technology Research Project of Jiangxi Education Department (GJJ200663).

Data availability

Data will be made available on reasonable request.

Declarations

Conflict of interest On behalf of all authors, the corresponding author states that there is no conflict of interest.

Ethical approval

This article does not contain any studies with human participants or animals performed by any of the authors.

References

1. J.D. Fontana, A. Souza, C.K. Fontana, I.L. Torriani, L. Farah, Acetobacter cellulose pellicle as a temporary skin substitute. Appl. Biochem. Biotechnol. **24–25**, 253–264 (1990)
2. D.A. Gregory, L. Tripathi, A.T.R. Fricker, E. Asare, I. Orlando, V. Raghavendran, I. Roy, Bacterial cellulose: a smart biomaterial with diverse applications. Curr. Opin. Biotechnol. **145**, 100623 (2021)
3. R.A.N. Pertile, S. Moreira, R.M. Gil da Costa, A. Correia, L. Guardao, F. Gartner, M. Vilanova, M. Gama, Bacterial cellulose: long-term biocompatibility studies, J. Biomater. Sci. Polym. Ed. **23**, 1339–1354 (2012).
4. H. Ullah, F. Wahid, H.A. Santos, T. Khan, Advances in biomedical and pharmaceutical applications of functional bacterial cellulose-based nanocomposites. Carbohydr. Polym. **150**, 330–352 (2016)
5. A. Svensson, E. Nicklasson, T. Harrah, B. Panilaitis, D.L. Kaplan, M. Brittberg, P. Gatenholm, Bacterial cellulose as a potential scaffold for tissue engineering of cartilage. Biomaterials **26**, 419–431 (2005)
6. S. Torgbo, P. Sukyai, Bacterial cellulose-based scaffold materials for bone tissue engineering. Appl. Mater. Today **11**, 34–49 (2018)
7. M. Zaborowska, A. Bodin, H. Backdahl, J. Popp, A. Goldstein, P. Gatenholm, Microporous bacterial cellulose as a potential scaffold for bone regeneration. Acta Biomater. **6**, 2540–2547 (2010)

8. C. Xu, J. Zhao, Q. Gong, S. Chen, Sustained release of vancomycin from bacterial cellulose membrane as dural substitutes for anti-inflammatory wound closure in rabbits. J. Biomater. Appl. **34**, 1470–1478 (2020)
9. A.N. Frone, D.M. Panaitescu, C.A. Nicolae, A.R. Gabor, R. Trusca, A. Casarica, P.O. Stanescu, D.D. Baciu, A. Salageanu, Bacterial cellulose sponges obtained with green cross-linkers for tissue engineering. Mater. Sci. Eng. C **110**, 110740 (2020)
10. N. Yin, M.D. Stilwell, T.M.A. Santos, H. Wang, D.B. Weibel, Agarose particle-templated porous bacterial cellulose and its application in cartilage growth in vitro. Acta Biomater. **12**, 129–138 (2015)
11. C. Gao, Y. Wan, C. Yang, K. Dai, T. Tang, H. Luo, J. Wang, Preparation and characterization of bacterial cellulose sponge with hierarchical pore structure as tissue engineering scaffold. J. Porous Mater. **18**, 139–145 (2011)
12. P.M. Favi, S.P. Ospina, M. Kachole, M. Gao, L. Atehortua, T.J. Webster, Preparation and characterization of biodegradable nano hydroxyapatite-bacterial cellulose composites with well-defined honeycomb pore arrays for bone tissue engineering applications. Cellulose **23**, 1263–1282 (2016)
13. Y. Hou, X. Wang, J. Yang, R. Zhu, Z. Zhang, Y. Li, Development and biocompatibility evaluation of biodegradable bacterial cellulose as a novel peripheral nerve scaffold. J. Biomed. Mater. Res. A **106**, 1288–1298 (2018)
14. J. Li, Y. Wan, L. Li, H. Liang, J. Wang, Preparation and characterization of 2,3-dialdehyde bacterial cellulose for potential biodegradable tissue engineering scaffolds. Mater. Sci. Eng. C **29**, 1635–1642 (2009)
15. H. Backdahl, M. Esguerra, D. Delbro, B. Risberg, P. Gatenholm, Engineering microporosity in bacterial cellulose scaffolds. J. Tissue Eng. Regener. Med. **2**, 320–330 (2008)
16. E. Bayir, E. Bilgi, E.E. Hames, A. Sendemir, Production of hydroxyapatite-bacterial cellulose composite scaffolds with enhanced pore diameters for bone tissue engineering applications. Cellulose **26**, 9803–9817 (2019)
17. G. Xiong, H. Luo, Y. Zhu, S. Raman, Y. Wan, Creation of macropores in three-dimensional bacterial cellulose scaffold for potential cancer cell culture. Carbohydr. Polym. **114**, 553–557 (2014)
18. T.R. Stumpf, X. Yang, J. Zhang, X. Cao, In situ and ex situ modifications of bacterial cellulose for applications in tissue engineering. Mater. Sci. Eng. C **82**, 372–383 (2018)
19. P. Cazon, M. Vazquez, Improving bacterial cellulose films by ex-situ and in-situ modifications: a review. Food Hydrocoll. **113**, 106514 (2021)
20. G. Xiong, H. Luo, C. Zhang, Y. Zhu, Y. Wan, Enhanced biological behavior of bacterial cellulose scaffold by creation of macropores and surface immobilization of collagen. Macromol. Res. **23**, 734–740 (2015)
21. J. Wang, Y.Z. Wan, H.L. Luo, C. Gao, Y. Huang, Immobilization of gelatin on bacterial cellulose nanofibers surface via crosslinking technique. Mater. Sci. Eng. C **32**, 536–541 (2012)
22. L. Xu, F. Ma, F.K.L. Leung, C. Qin, W.W. Lu, B. Tang, Chitosan-strontium chondroitin sulfate scaffolds for reconstruction of bone defects in aged rats. Carbohydr. Polym. **273**, 118532 (2021)
23. S. Yan, Q. Zhang, J. Wang, Y. Liu, S. Lu, M. Li, D. Kaplan, Silk fibroin/chondroitin sulfate/hyaluronic acid ternary scaffolds for dermal tissue reconstruction. Acta Biomater. **9**, 6771–6782 (2013)
24. M. Pezeshki-Modaress, H. Mirzadeh, M. Zandi, S. Rajabi-Zeleti, N. Sodeifi, N. Aghdami, M.R.K. Mofrad, Gelatin/chondroitin sulfate nanofibrous scaffolds for stimulation of wound healing: In-vitro and in-vivo study. J. Biomed. Mater. Res. **105**, 2020–2034 (2017)
25. H. Cao, S.-Y. Xu, EDC/NHS-crosslinked type II collagen-chondroitin sulfate scaffold: characterization and in vitro evaluation, J. Mater. Sci.: Mater. Med. **19**, 567–575 (2008).
26. S. Chen, W. Chen, Y. Chen, X. Mo, C. Fan, Chondroitin sulfate modified 3D porous electrospun nanofiber scaffolds promote cartilage regeneration. Mater. Sci. Eng. C **118**, 11312 (2021)
27. J.Y. Lai, Y.T. Li, C.H. Cho, T.C. Yu, Nanoscale modification of porous gelatin scaffolds with chondroitin sulfate for corneal stromal tissue engineering. Int. J. Nanomed. **7**, 1101–1114 (2012)
28. A. Sadeghi, M. Zandi, M. Pezeshki-Modaress, S. Rajabi, Tough, hybrid chondroitin sulfate nanofibers as a promising scaffold for skin tissue engineering. Int. J. Biol. Macromol. **132**, 63–75 (2019)
29. K. Xu, Z. Wang, J.A. Copland, R. Chakrabarti, S.J. Florczyk, 3D porous chitosan-chondroitin sulfate scaffolds promote epithelial to mesenchymal transition in prostate cancer cells. Biomaterials **254**, 120126 (2020)
30. G. M. de Olyveira, P. Basmaji, L. M. Manzine Costa, M.L. dos Santos, C. d. S. Riccardi, F. P. Semeghini Guastaldi, R.M. Scarel-Caminaga, T. S. de Oliveira Capote, E. Pizoni, A. C. Guastaldi, Surface physical chemistry properties in coated bacterial cellulose membranes with calcium phosphate, Mater. Sci. Eng. C **75**, 1359–1365 (2017).
31. G. M. de Olyveira, M.L. dos Santos, C. d. S. Riccardi, L. M. Manzine Costa, P. B. Daltro, P. Basmaji, G. d. C. Daltro, A. C. Guastaldi, Physically Modified Bacterial Cellulose Biocomposites for Guided Tissue Regeneration, Sci. Adv. Mater. **7**, 1657–1664 (2015).
32. G. Helenius, H. Bäckdahl, A. Bodin, U. Nannmark, P. Gatenholm, B. Risberg, In vivo biocompatibility of bacterial cellulose. J. Biomed. Mater. Res. A **76A**, 431–438 (2006)
33. K.J. Burg, S. Porter, J.F. Kellam, Biomaterial developments for bone tissue engineering. Biomaterials **21**, 2347–2359 (2000)
34. L. Liang, T. Hou, Q. Ouyang, L. Xie, S. Zhong, P. Li, S. Li, C. Li, Antimicrobial sodium alginate dressing immobilized with

polydopamine-silver composite nanospheres. Compos. Part B **188**, 107877 (2020)

35. L. Gu, T. Li, X. Song, X. Yang, S. Li, L. Chen, P. Liu, X. Gong, C. Chen, L. Sun, Preparation and characterization of methacrylated gelatin/bacterial cellulose composite hydrogels for cartilage tissue engineering. Regener. Biomater. **7**, 1–8 (2019)
36. J. Wu, N. Yin, S. Chen, D. Weibel, H. Wang, Simultaneous 3D cell distribution and bioactivity enhancement of bacterial cellulose (BC) scaffold for articular cartilage tissue engineering. Cellulose **26**, 1–16 (2019)
37. C. Castro, A. Vesterinen, R. Zuluaga, G. Caro, I. Filpponen, O.J. Rojas, G. Kortaberria, P. Ganan, In situ production of nanocomposites of poly(vinyl alcohol) and cellulose nanofibrils from gluconacetobacter bacteria: effect of chemical crosslinking. Cellulose **21**, 1745–1756 (2014)
38. G. Zhu, H. Wang, H. Xu, L. Zhang, Enhanced capacitive deionization by nitrogen-doped porous carbon nanofiber aerogel derived from bacterial-cellulose. J. Electroanal. Chem. **822**, 1–37 (2018)
39. Y. Liu, H. Lv, L. Ren, G. Xue, Y. Wang, Improving the moisturizing properties of collagen film by surface grafting of chondroitin sulfate for corneal tissue engineering. J. Biomater. Sci. Polym. Ed. **27**, 758–772 (2016)
40. T. Fan, J. Chen, P. Pan, Y. Zhang, Y. Hu, X. Liu, X. Shi, Q. Zhang, Bioinspired double polysaccharides-based nanohybrid scaffold for bone tissue engineering. Colloids Surf. B **147**, 217–223 (2016)
41. Y. Gong, Y. Zhu, Y. Liu, Z. Ma, C. Gao, J. Shen, Layer-by-layer assembly of chondroitin sulfate and collagen on aminolyzed poly(l-lactic acid) porous scaffolds to enhance their chondrogenesis. Acta Biomater. **3**, 677–685 (2007)
42. Y. Wan, S. Yang, M. Peng, M. Gama, Z. Yang, X. Deng, J. Zhou, C. Ouyang, H. Luo, Controllable synthesis of biomimetic nano/submicro-fibrous tubes for potential small-diameter vascular grafts. J. Mater. Chem. B **8**, 5694–5706 (2020)
43. H. Luo, J. Dong, X. Xu, J. Wang, Z. Yang, Y. Wan, Exploring excellent dispersion of graphene nanosheets in three-dimensional bacterial cellulose for ultra-strong nanocomposite hydrogels. Compos. Part A Appl. Sci. Manuf. **109**, 290–297 (2018)
44. X. Yang, K. Shi, I. Zhitomirsky, E.D. Cranston, Cellulose nanocrystal aerogels as universal 3D lightweight substrates for supercapacitor materials. Adv. Mater. **27**, 6104–6109 (2015)
45. H. Sehaqui, M. Salajkova, Q. Zhou, L.A. Berglund, Mechanical performance tailoring of tough ultra-high porosity foams prepared from cellulose I nanofiber suspensions. Soft Matter **6**, 1824–1832 (2010)
46. R. T. Olsson, M. A. S. Azizi Samir, G. Salazar Alvarez, L. Belova, V. Strom, L. A. Berglund, O. Ikkala, J. Nogues, U. W. Gedde, Making flexible magnetic aerogels and stiff magnetic nanopaper using cellulose nanofibrils as templates, Nat. Nanotechnol. **5**, 584–588 (2010).
47. H. Luo, Y. Zhang, G. Li, J. Tu, Z. Yang, G. Xiong, Z. Wang, Y. Huang, Y. Wan, Sacrificial template method for the synthesis of three-dimensional nanofibrous 58S bioglass scaffold and its invitro bioactivity and cell responses. J. Biomater. Appl. **32**, 265–275 (2017)
48. H. Luo, Y. Zhang, Z. Wang, Z. Yang, J. Tu, Z. Liu, F. Yao, G. Xiong, Y. Wan, Constructing three-dimensional nanofibrous bioglass/gelatin nanocomposite scaffold for enhanced mechanical and biological performance. Chem. Eng. J. **326**, 210–221 (2017)
49. J. Ran, P. Jiang, S. Liu, G. Sun, P. Yan, X. Shen, H. Tong, Constructing multi-component organic/inorganic composite bacterial cellulose-gelatin/hydroxyapatite double-network scaffold platform for stem cell-mediated bone tissue engineering. Mater. Sci. Eng. C **78**, 130–140 (2017)
50. P. Jiang, J. Ran, P. Yan, L. Zheng, X. Shen, H. Tong, Rational design of a high-strength bone scaffold platform based on in situ hybridization of bacterial cellulose/nano-hydroxyapatite framework and silk fibroin reinforcing phase. J. Biomater. Sci. Polym. Ed. **29**, 107–124 (2018)
51. P. Basu, N. Saha, R. Alexandrova, P. Saha, Calcium phosphate incorporated bacterial cellulose-polyvinylpyrrolidone based hydrogel scaffold: structural property and cell viability study for bone regeneration application. Polymers (Basel) **11**(11), 1821 (2019)
52. Y. Li, X. Xun, Y. Xu, A. Zhan, E. Gao, F. Yu, Y. Wang, H. Luo, C. Yang, Hierarchical porous bacterial cellulose scaffolds with natural biomimetic nanofibrous structure and a cartilage tissue-specific microenvironment for cartilage regeneration and repair. Carbohydr. Polym. **276**, 118790 (2022)
53. X. Xun, Y. Li, X. Zhu, Q. Zhang, Y. Lu, Z. Yang, Y. Wan, F. Yao, X. Deng, H. Luo, Fabrication of robust, shape recoverable, macroporous bacterial cellulose scaffolds for cartilage tissue engineering. Macromol Biosci **21**, e2100167 (2021)
54. M. Kouhi, J. Varshosaz, B. Hashemibeni, A. Sarmadi, Injectable gellan gum/lignocellulose nanofibrils hydrogels enriched with melatonin loaded forsterite nanoparticles for cartilage tissue engineering: fabrication, characterization and cell culture studies. Mater. Sci. Eng. C **115**, 111114 (2020)
55. B. Zhang, J. Huang, R.J. Narayan, Gradient scaffolds for osteochondral tissue engineering and regeneration. J. Mater. Chem. B **8**, 8149–8170 (2020)
56. Y. Zhang, X. Liu, L. Zeng, J. Zhang, J. Zuo, J. Zou, J. Ding, X. Chen, Polymer fiber scaffolds for bone and cartilage tissue engineering. Adv. Funct. Mater. **29**, 1903279 (2019)
57. F. Hejazi, S. Bagheri-Khoulenjani, N. Olov, D. Zeini, A. Solouk, H. Mirzadeh, Fabrication of nanocomposite/nanofibrous functionally graded biomimetic scaffolds for osteochondral tissue regeneration. J. Biomed. Mater. Res. A **109**, 1657–1669 (2021)
58. H. Luo, G. Xiong, C. Zhang, D. Li, Y. Zhu, R. Guo, Y. Wan, Surface controlled calcium phosphate formation on

three-dimensional bacterial cellulose-based nanofibers. Mater. Sci. Eng. C **49**, 526–533 (2015)
59. N.V. Lukasheva, D.A. Tolmachev, Cellulose nanofibrils and mechanism of their mineralization in biomimetic synthesis of hydroxyapatite/native bacterial cellulose nanocomposites: molecular dynamics simulations. Langmuir **32**, 125–134 (2016)
60. F. Nurlidar, E. Budianto, D. Darwis, Hydroxyapatite deposition on modified bacterial cellulose matrix. Macromol. Symp. **353**, 128–132 (2015)
61. B. Sun, F. Wei, W. Li, X. Xu, H. Zhang, M. Liu, J. Lin, B. Ma, C. Chen, D. Sun, Macroporous bacterial cellulose grafted by oligopeptides induces biomimetic mineralization via interfacial wettability. Colloids Surf. B **183**, 110457 (2019)
62. Y.Z. Wan, Y. Huang, C.D. Yuan, S. Raman, Y. Zhu, H.J. Jiang, F. He, C. Gao, Biomimetic synthesis of hydroxyapatite/bacterial cellulose nanocomposites for biomedical applications. Mater. Sci. Eng. C **27**, 855–864 (2007)
63. Y. Wan, Z. Lin, Q. Zhang, D. Gan, M. Gama, J. Tu, H. Luo, Incorporating graphene oxide into biomimetic nano-microfibrous cellulose scaffolds for enhanced breast cancer cell behavior. Cellulose **27**, 4471–4485 (2020)
64. H. Luo, D. Gan, M. Gama, J. Tu, F. Yao, Q. Zhang, H. Ao, Z. Yang, J. Li, Y. Wan, Interpenetrated nano-and submicro-fibrous biomimetic scaffolds towards enhanced mechanical and biological performances. Mater. Sci. Eng. C: Mater. Biol. Appl. **108**, 110416 (2020)
65. Z. Wang, Y. Cui, J. Wang, X. Yang, Y. Wu, K. Wang, X. Gao, D. Li, Y. Li, X.-L. Zheng, The effect of thick fibers and large pores of electrospun poly (ε-caprolactone) vascular grafts on macrophage polarization and arterial regeneration. Biomaterials **35**, 5700–5710 (2014)
66. A. H. Aparecida, M. V. L. Fook, A. C. Guastaldi, Biomimetic apatite formation on Ultra-High Molecular Weight Polyethylene (UHMWPE) using modified biomimetic solution, J. Mater. Sci.: Mater. Med. **20**, 1215–1222 (2009).